Upper Ocean Thermal Structure and the

Western North Pacific Category-5 Typhoons

Part I: Ocean Features and Category-5 Typhoon's Intensification

I-I Lin*, Chun-Chieh Wu*, Iam-Fei Pun*, and Dong-Shan Ko~

*Dept. of Atmospheric Sciences, National Taiwan University, Taipei, Taiwan

~ Naval Research Laboratory, Stennis Space Center, Mississippi, USA

Corresponding author address: Dr. I-I Lin, Dept. of Atmospheric Sciences, National Taiwan University, No. 1, Sec. 4, Roosevelt Rd., Taipei 106, Taiwan; e-mail: iilin@as.ntu.edu.tw

Abstract

Category-5 cyclones are the most intense and devastating cyclones on earth. With increasing observations of category-5 cyclones, such as Hurricane Katrina (2005), Rita (2005), Mitch (1998), and Supertyphoon Maemi (2003) found to intensify on warm ocean features (i.e., regions of positive sea surface height anomalies detected by satellite altimeters), there are great interests in investigating the role ocean features play in the intensification of category-5 cyclones. Based on 13 years' of satellite altimetry data, *in situ* and climatological upper ocean thermal structure data, best track typhoon data of the US Joint Typhoon Warning Center, together with an ocean mixed layer model, 30 western North Pacific category-5 typhoons occurred during the typhoon season from 1993 to 2005 are systematically examined in this study.

Two different types of situations are found. The first type is the situation found in the western North Pacific South Eddy Zone (127-170°E, 21-26°N) and the Kuroshio (127-170°E, 21-30°N) region. In these regions, the background climatological warm layer is relatively shallow (typically the depth of the 26°C isotherm is around 60m and upper ocean heat content ~ 50 kj cm^{-2}). Therefore passing over positive features is critical to meet the ocean's part of necessary condition in intensification because the features can effectively deepen the warm layer (depth of the 26°C isotherm reaching 100m and upper ocean heat content ~ 110 kj cm^{-2}) to restrain typhoon's self-induced ocean cooling. In the past 13 years, 8 out of the 30 category-5 typhoons (i.e., 27%) belong to this situation.

The second type is the situation found in the gyre central region (121-170°E, 10-21°N) where the background climatological warm layer is deep (typically the depth of the 26°C isotherm ~ 105-120m and upper ocean heat content ~ 80-120 kj cm^{-2}). In this deep, warm background, passing over positive features is not critical since the background itself is already sufficient to restrain the self-induced cooling negative feedback during intensification.

1. Introduction

a. Motivation

Category-5[1] (1-min (10-min) maximum sustained wind speed > 71 (65) m/s) tropical cyclones, Hurricane Katrina (2005) and Supertyphoon Maemi (2003) for instance, are the most intense and destructive cyclones on earth.   Given their huge impact, it is important to understand why these storms can reach such extraordinary intensity. However, much remains unclear as cyclone's intensification is a highly complex process involving the interaction of the atmosphere, ocean, and cyclone's own structure (Gray 1979; Holliday and Thompson 1979; Emanuel 1986, 2000, 2006; Shay et al. 2000; Kaplan and DeMaria 2003; Wang and Wu 2003; Emanuel et al. 2004; Lin et al. 2005; Houze et al. 2007; Pun et al. 2007; Wu et al. 2007). In exploring ocean's role in cyclone's intensification, it is necessary to consider not only sea surface temperature (SST), but the thermal structure of the upper ocean column because cyclones interact not only just with the surface, but with the upper ocean layer (typically from surface down to 100-200m) (Gray 1979; Holliday and Thompson 1979; Emanuel 1986; Shay et al. 2000; Goni and Trinanes 2003; Lin et al. 2003a, b; Emanuel et al. 2004; Lin et al. 2005; Scharroo et al. 2005; Pun et al. 2007; Wu et al. 2007). This is especially true for category-5 cyclones since the more intense the wind is, the deeper the ocean mixing is involved (Price 1981; Bender and Ginis 2000; Pun et al. 2007).

However, it has been difficult to explore the UOTS (upper ocean thermal structure) related issues due to the lack of subsurface observations, over the vast oceans, especially in TC conditions (Gray 1979; Holliday and Thompson 1979; Emanuel 1986; Shay et al. 2000; Goni and Trinanes 2003; Emanuel et al. 2004; Lin et al. 2005; Scharroo et al. 2005).   With the advancement in remote sensing (e.g., satellite altimetry, Fu et al. 1994) and *in situ* ocean measurements (e.g., ARGO floats, Gould et al. 2004), it is now possible to study this subject with more reliable new observations. To conduct a systematic study, it is needed to have as many category-5 cyclone cases stretching for as longer period as possible.   In this

---

[1] Saffir-Simpson Tropical Cyclone Scale based on the 1-minute (10-minute) maximum sustained winds: Category-1: 34-43 (30-37) ms^{-1}, Category-2: 44-50 (38-43) ms^{-1}, Category-3: 51-59 (44-51) ms^{-1}, Category-4: 59-71 (52-61) ms^{-1}, and Category-5: > 71 (> 61) ms^{-1}.

work, the western North Pacific Ocean[2] is chosen for investigation because it is among the world oceans where most number of categoty-5 cyclones (i.e. typhoons) are found (Holliday and Thompson 1979; Emanuel 1986). This work is presented in a series of two papers.   In Part I (this paper), the role ocean features play in category-5 typhoon's intensification is studied.   In Part II, issues on translation speed and geographical dependence related to UOTS are explored.

b. Issues on the interaction between ocean features and category-5 tropical cyclones

Due to the presence of mesoscale ocean eddies, along with the change in the location of the currents, and the large-scale variability (e.g., El Niño), there exist many dynamic ocean features in certain high-impact tropical cyclone basins, such as the Gulf of Mexico and the western North Pacific Ocean (Wyrtki 1979; Philander 1990; Qiu 1999; Johnson et al. 2000; Shay et al. 2000; Roemmich and Gilson 2001; Goni and Trinanes 2003; Hwang et al. 2004; Emanuel et al. 2004; Lin et al. 2005; Scharroo et al. 2005; Oey et al. 2006).   Since these dynamic features are perturbations from the climatology, they are generally not observable from the ocean climatological data (Stephens et al. 2002).   With the advance in the remote sensing, these features nowadays can be effectively detected by satellite altimeters (Fu et al., 1994) as regions of positive or negative sea surface height anomalies (SSHA) (Goni et al. 1996; Qiu 1999; Shay et al. 2000; Goni and Trinanes 2003; Emanuel et al. 2004; Hwang et al. 2004; Lin et al. 2005; Pun et al. 2007).   Positive-SSHA features (also refer to as warm features) are regions where warm upper ocean layer (warm ocean layer is often defined as from surface down to the depth of the 26°C isotherm, i.e., D26) (Leipper and Volgenau 1972; Shay et al. 2000) is deeper than climatology, i.e., regions with increase warm layer thickness from the climatological thickness. On the other hand, negative-SSHA features are regions where warm upper ocean layer shoals from climatology and are regions where warm layer thickness decreases (Qiu 1999; Shay et al. 2000; Goni and Trinanes 2003; Hwang et al. 2004; Lin et al. 2005; Scharroo 2005; Pun et al. 2007). Besides from D26, Tropical Cyclone Heat Potential or Upper

---

[2] From the best-track data of Joint Typhoon Warning Center during 1960-2005, in average 2.5 typhoons reach the category-5 intensity in the western North Pacific Ocean each year.

Ocean Heat Content (UOHC, i.e., the integrated heat content from the depth of the 26°C isotherm to the surface) is another parameter which is often used in characterizing these features whereby in the positive (negative) features, the UOHC is higher (lower) than the climatological value (Leipper and Volgenau 1972; Shay et al. 2000; Goni and Trinanes 2003; Pun et al. 2007; Wada and Usui 2007). Also, it should be noted that these features are usually not differentiable by their SSTs but by the subsurface-related parameters (i.e., D26 or UOHC) since these features represent subsurface variabilities (Goni et al. 1996; Shay et al. 2000; Goni and Trinanes 2003; Lin et al. 2005; Pun et al. 2007).

Recent observations find that a notable number of category-5 cyclones, such as Hurricane Katrina (2005) (Scharroo et al. 2005), Rita (2005), Mitch (1998) (Emanuel et al. 2004), Supertyphoon Maemi (2003) (Lin et al. 2005), and Dianmu (2004) (Pun et al. 2007) intensified rapidly (Kaplan and DeMaria 2003) into the fifth category while they were moving over the positive-SSHA features. From this regard, the interaction between ocean features and category-5 cyclones is worth of being examined. Note that most exiting works (Shay et al. 2000; Goni and Trinanes 2003; Emanuel et al. 2004; Lin et al. 2005; Scharroo et al. 2005; Pun et al. 2007) on this issue are based on case study of individual events. It is not clear whether more generalized conclusions can be deduced about the relation between the category-5 cyclones and their passage over the positive-SSHA features. In this study, all category-5 typhoons (in total 30 cases) that occurred during the May-October typhoon season from 1993 to 2005 (i.e., 13 years) are studied, since the main satellite instrument for observation, the TOPEX/Poseidon altimeter (Fu et al. 1994) became available starting from 1993. In Section 2, the hydrographical setting in the western North Pacific, including the origin of the features and background climatology, is introduced. The data and methodology are presented in Section 3. Results, discussions, and conclusions are given in Sections 4-6.

2. Hydrographic setting in the western North Pacific

a. Origin of the features

Over the western North Pacific, abundant positive and negative-SSHA features are present all year round, as clearly observed from the satellite altimetry SSHA maps (Fig. 1) (Qiu 1999; Hwang et al. 2004;

Lin et al. 2005). In the northern part (135-170°E, 30-37°N), the features are often mesoscale features associated with the Kuroshio rings (Yasuda et al. 1992). These features are originated from the western boundary currents (Richard 1981; Pickard and Emery 1990; Yasuda et al. 1992) and are similar to the Gulf Stream rings (Shay et al. 2000). In the central part (127-170°E, 21-26°N), features are associated with mesoscale eddies originated from the baroclinic instability of the weak flow between the westward North Equatorial Current and the eastward Subtropical Countercurrent (Qiu 1999; Roemmich and Gilson 2001). These 2 eddy-rich regions are commonly known as the north and the south eddy zone (NEZ and SEZ) (Fig. 1) (Qiu 1999; Roemmich and Gilson 2001; Hwang et al. 2004; Lin et al. 2005). To the west of the SEZ is the Kuroshio (121-127°E, 21-30°N) warm current region where features are caused by Kuroshio's variability (Qiu 1999). Moving southward to the region near 121-170°E, 10-21°N is the center part of the western subtropical gyre (referred to as the gyre central region in this study), where large, basin scale features are found. These features are usually affected by large-scale processes, such as the El Niño (Wyrtki 1979; Philander 1990; Johnson et al. 2000). For example, during the El Niño period in October 1997, a large negative-SSHA feature (< -20cm) is observed in the gyre central (Fig. 1b), while in June, 2004, a positive-SSHA feature is found (Fig. 1a).

b. Background climatology

With these features, the background climatological UOTS in the western North Pacific is constantly modulated. The background summer UOTS, in SST and the depth of the 26°C isotherm (D26), is illustrated for reference in Figs. 2a and b, respectively. As shown in the July-September averaged SST map from the TRMM (Tropical Rainfall Measuring Mission, Wentz et al., 2000) satellite during 2000-2005 (Fig. 2a), due to the strong solar radiation in summer, uniformly warm SST of $\geqq 28$°C covers most part of the western North Pacific ocean (Fig. 2a). As for the corresponded D26 (data from the NOAA/World Ocean Atlas 2001, Stephens et al. 2002) (Fig. 2b), the mean thickest water lies in the gyre central region (121-170°E, 10-21°N) with D26 in the range of 80-130 m. In contrast, the thickness in

the South China Sea (105-120°E, 5-20°N) of the similar latitude is only about 20-70 m.   In the northern

part of the gyre, i.e., in the SEZ (127-170°E, 21-26°N), it is found that the climatological D26 shoals

significantly northwards from 70 to 40 m.   In the Kuroshio warm current region (121-127°E, 21-30°N),

the mean D26 is between 50 and 80 m.   To the further north, the background D26 reduces to below 20m

at 30°N in the NEZ region.

3. Data and methodology

In this work, the best-track data from the JTWC are used.   The SST data used is from the TRMM

satellite (Wentz et al. 2000).   Two satellite altimeters, i.e., the TOPEX/Poseidon (starting from 1993) and

JASON-1 (from 2002), are utilized to detect ocean features (Fu et al. 1994). The altimetry data used is the

GDR (Geophysical Data Record) product from the NASA Jet Propulsion Laboratory (JPL). The accuracy

in sea surface height measurement is 3.3 cm and the nominal along-track spatial resolution is 7km (see

http://podaac.jpl.nasa.gov/jason/documents/). For the 1993-2001 cases, TOPEX/Poseidon altimetry data

is used. As for the 2002-2005 cases, JASON-1 data is added so as to maximize data usage. The

corresponding maximum swath gap for single altimeter usage is 300km and 150km if 2 altimeters are

used. For each typhoon case, pre-typhoon SSHA map from a 10-day altimetry cycle (gridded to 1/4° from

the along track data) is used to identify the primary ocean feature (i.e., the feature type which typhoon

encounter for the longest time during intensification).   Here the intensification period is defined as from

the category-1 to the peak category-5 intensity.   Three categories of primary features are defined as

follows: positive-SSHA feature (averaged SSHA > 6 cm), negative-SSHA feature (averaged SSHA < 6

cm), and no-feature condition (averaged SSHA between -6 and 6 cm) (Fu et al. 1994; Qiu 1999; Shay et

al. 2000; Goni and Trinanes 2003; Hwang et al. 2004; Lin et al. 2005; Pun et al. 2007).

To assess the detail upper ocean thermal structure, the available *in situ* near co-incident/co-located

upper ocean thermal structure profiles from the ARGO float (Gould et al. 2004) and the NOAA/GTSPP

(Global Temperature and Salinity Profile Program) data base (Keeley et al. 2003) are cross-examined for

each case.   All profiles are acquired within 1 week prior to the passage of the typhoon.   Among the 30 cases, *in situ* profiles were identified in 11 cases. Most of the profiles are located on the track or within 0.5° from the storm center while profiles for 3 cases are around 1.5 to 2 degrees from the track. By comparing the *in situ* profiles with the climatological profiles (from the NOAA/World Ocean Atlas 2001, WOA01) (Stephens et al. 2002) along the storm tracks, the deepening and shoaling of D26 caused by the features can be assessed. Also upper ocean heat content (i.e. UOHC or Q_H)[3] is calculated for each *in situ* and climatological profile so as to assess the increase (or decrease) in UOHC due to the presence of features.

To estimate ocean's negative feedback to intensity from typhoon's self-induced ocean cooling (Price, 1981; Emanuel, 1999; Bender and Ginis, 2000; Cione and Uhlhorn, 2003), the Price-Weller-Pinkel ocean mixed layer model (Price et al. 1986; Jacob et al. 2000; Jacob and Shay 2003; Lin et al. 2003b) is used. The searched pre-typhoon *in situ* profiles in the features are adopted as initial profiles. Another reference set of initial profiles used are the background climatological profiles (Stephens et al., 2002); so as to estimate the self-cooling under climatological condition. For each profile, the storm-induced cooling is estimated progressively with increase in wind forcing from category-1 to 5, according to the Saffir-Simpson scale.   The 10-minute average maximum sustained wind, ranging from 30-65 m s^{-1}, for every 5 m s^{-1} interval, is used to drive the model.   The drag coefficient (C_d) from Powell et al. (2003) is used as the coefficient under the cyclone-wind condition.

Experiments are run under various translation speeds *(U_h)*, since the typhoon-induced SST cooling is not only a function of wind speed, but also a function of the translation speed (U_h); i.e., the faster the storm moves, the less the SST cooling is induced (Price 1981). As shown in Fig. 3, in the simulation, a parameter, $TC_{transit-time}$, is calculated as $TC_{transit-time} = D / U_h$ (1) where D represents the inner core

---

[3] $Q_H(x, y, t) = c_p \rho \Delta T(x, y, z, t) \Delta Z$, where c_p is the capacity heat of the water at constant pressure taken as 4178 J kg^{-1}℃$^{-1}$, ρ is the average density of the upper ocean taken as 1026 kg m^{-3}, and ΔT is the difference between $T(z)$ and 26℃ over the depth interval (ΔZ).

diameter. Thus, $TC_{transit-time}$ is the time needed for the inner core of typhoon to pass over a specific point location in the ocean (Cione and Uhlhorn 2003). Therefore, for each point location, the mixed layer model is run according to the $TC_{transit-time}$. The inner core diameter D is defined as 220 km in this work because the western North Pacific typhoons are generally ~ 1.2-1.4 times the size of the Atlantic hurricanes (Merrill 1984; Liu and Chan 1999) and the reported mean inner core diameter for the Atlantic hurricanes is 180km (Cione and Uhlhorn 2003).

In this work, the threshold criterion from Emanuel (1999) is adopted, i.e., the self-induced SST cooling exceeding 2.5°C is regarded as unsuitable condition for intensification, because such cooling would be sufficient to shut down the entire energy production of a storm (Gallacher et al. 1989; Emanuel 1999; Emanuel et al. 2004). To further substantiate this, air-sea sensible and latent heat flux is estimated and is discussed in Section 5.2.   Finally, since Price et al. (1986) is a simple 1-D mixed layer model, in the discussion section (Sec. 5.3), a 3-D numerical experiment is run using US Naval Research Lab (NRL)'s EASNFS ocean model (Ocean/Nowcast Forecast System for the East Asian Seas) (Ko et al. 2003; Chapman et al. 2004) to discuss the possible difference between 1-D and 3-D simulations related to this work (Jacob et al. 2000; Jacob and Shay 2003).

4. Results

Fig. 4 depicts the full track (in grey) and the intensification track segments (in red, i.e., during the intensification period from category-1 to the peak category-5 intensity) for the 30 cases.   Even though the full tracks of typhoons cover the entire western North Pacific region, it can be found that the intensification process only occurs while the storms are located in the south eddy zone (127-170°E, 21-26°N), the gyre central (121-170°E, 10-21°N), and the southern part of the Kuroshio region (121-127°E, 21-26°N).   Among the 30 cases, 7 storms peak in the south eddy zone (Table 1), 22 peak in the gyre central (Table 3), and 1 peak in the Kuroshio region (Table 5).   The results are presented as follows.

a. The south eddy zone cases: positive SSHA features

Fig. 5 depicts the SSHA features the typhoons encounter during intensification for the 7 cases at the SEZ. It is found that the SSHA features in all these 7 cases are positive cases. As shown in Figs. 5b and f, some typhoons are observed to intensify all the way from category-1 to 5 when passing over these positive-SSHA features. The intensification of the other cases (e.g., Figs. 5a,c,d,e,g) is similar to the processes associated with those well-known category-5 cases in the Atlantic/Gulf of Mexico. For example, Mitch (1998) and Katrina (2005) that all passed over positive-SSHA features for a considerable period of time (typically intensified for more than 2 categories) during their intensification (Emanuel et al. 2004; Lin et al. 2005; Scharroo et al. 2005).

Based on the *in situ* profiles (red profiles in Fig. 6) in these features (locations depicted in Figs. 5b, f, and g), it is shown that the region with positive-SSHA features contains the warm water extending much deeper than that under the climatological condition (black profiles in Fig. 6). As summarized in Table 2, both D26 and UOHC increase significantly. In the positive feature regions, D26 reaches as deep as 90-120 m whereas the climatological D26 is only around of 40-65 m while UOHC also increases significantly from an average of 47 to 109 kj cm^{-2} (i.e., > 100% increase) (Table 2).

With this large increase in the warm layer thickness and UOHC, the corresponding impact in storm-induced SST cooling is assessed. The storm-induced SST cooling estimation averaged over all climatological profiles (black profiles in Fig. 6) under 10 different translation speeds (i.e., U_h =1, 2, 3…to 10 m s^{-1}) are depicted in Fig. 7a. The estimations based on the *in situ* profiles in the positive-SSHA features (red profiles in Fig. 6) are depicted in Fig. 7b. In these figures, regions of storm-induced SST cooling exceeding the 2.5°C threshold are shaded, indicating the unfavorable condition for intensification (Emanuel 1999). The comparison of Figs. 7a and b shows that under the same translation speed and wind forcing (x-axis), the storm-induced SST cooling (y-axis) is evidently larger under the climatological condition (Fig. 7a) than under the condition with the positive-SSHA features (Fig. 7b). As an example,

10

for a typhoon moving at $U_h = 5$ m s^{-1} and with 60 m s^{-1} wind speed, the averaged storm-induced cooling is 2.6°C under the climatological condition (green curve in Fig. 7a).   However, under the positive-SSHA situation, the corresponding SST cooling is only around 1.0°C (green curve in Fig. 7b).   This clearly shows that the storm-induced SST cooling are limited in the area with the positive-SSHA features (Cione and Uhlhorn2003; Lin et al. 2005).

During the intensification period for these 7 cases over the SEZ (Table 1), the observed storm translation speeds are in the range between 3.0 and 5.3 m s^{-1}.   Given this range of translation speeds in Fig. 7a, the corresponding storm-induced SST cooling starts to fall into the shaded region for category-3 (i.e., the orange curve for $U_h = 3$ m s^{-1} in Fig. 7a) or category-4 typhoons (i.e., the light blue and green curves for $U_h = 4$ and 5 m s^{-1} in Fig. 7a). As in Fig. 7a, one sees that at category-4, the self-induced cooling can already reach as much as 3.5°C, indicating unfavorable condition for continual intensification (i.e., no more energy supply, Gallacher et al. 1989; Emanuel 1999) to the fifth category under the climatological condition in the SEZ.   As ocean is a necessary condition in intensification (Holliday and Thompson 1979; Emanuel 1986), this shows that it is not possible to support intensification to category-5 under the climatogical upper ocean thermal structure in the SEZ, even if other conditions (e.g., atmosphere) are favorable.

However, under the positive-SSHA feature situation, the corresponding storm-induced SST cooling at this observed range of translation speeds is much smaller.   As seen in Fig. 7b, given $U_h = 3$, 4, and 5 m s^{-1}, storm-induced SST cooling never falls into the shaded region throughout the intensification period from category-1 to 5.   Even with the intense 65 m s^{-1} wind, the storm-induced SST cooling is still only around 1.2°C when traveling at $U_h = 5$ m s^{-1} (green curve in Fig. 7b).   These results explain why all SEZ cases in the past 13 years all passed over positive features because the presence of the positive-SSHA features can effectively suppress the self-induced cooling. Otherwise, it will not be possible to satisfy the ocean's necessary condition under the climatological UOTS in the SEZ.

b.   Cases in the gyre central region

Table 3 and Fig. 8 summarize the primary features in the gyre central region the 22 cases of typhoons encountered while intensifying to the fifth category.   It is found that the intensification of typhoons to category 5 not only exists when they are over the positive-SSHA features (e.g., Figs. 8b and s), but also on the normal (i.e., no primary features, e.g., Figs. 8f and t) and even negative SSHA features (e.g. Figs. 8i-k).   As summarized in Table 3, among the 22 gyre cases, 17 typhoons belong to the positive-SSHA feature scenario, 2 of the normal scenario, and 3 of the negative-SSHA feature scenario. These 3 different scenarios are discussed.

(1)   Negative-SSHA features scenario

As in Figs. 8i-k, 3 category-5 typhoons were observed to intensify to the fifth cateogory while passing the negative-SSHA features (SSHA ~ -10 to -30cm). In the positive-SSHA scenario, the warm layer thickness is larger than the climatoloigcal thickness (Shay et al. 2000; Goni and Trinanes 2003; Emanuel et al. 2004; Lin et al. 2005; Pun et al. 2007), hence it is understandable that with increase in the warm layer thickness, intensification is even more favorable. However, the negative-SSHA scenario is the opposite, the warm layer shoals and the warm layer thickness is smaller than the climatological thickness. So one would wonder why under such shoaling situation the storm would still intensify to the fifth category.

Comparing the *in situ* profiles in the negative-SSHA features (green profiles in Fig. 9a, profile locations depicted in Fig. 8j, Table 4) with the climatological profiles in the gyre central region for these negative-SSHA cases (black profiles in Fig. 9a), one sees that the D26 shoals from the climatological value of 105m to 67-74m, i.e., an average decrease of the warm layer thickness by 35m (Table 4a) and UOHC from 103 to 80 kj cm^{-2}.   It should be noted that the observed negative-SSHA features have the thermal structure with the shallower warm layer, but not the reduced SST.   As in Fig. 9a and Table 4a, both climatological and the *in situ* SST show the very warm SST of around 29°C. In other words, the

12

negative-SSHA features indicate a 'shallower' warm layer situation, but not a 'reduced SST' situation.

As for the corresponding storm-induced SST cooling, more pronounced cooling is expected when the storm is over the negative-SSHA feature (Fig. 10b) than under the climatological condition (Fig. 10a). Note that the storm-induced SST cooling falls to the shaded region only when $U_h = 1 - 2$ m s^{-1} under climatology (purple and pink curves in Fig. 10a). On the other hand, when over the negative-SSHA features, the cooling falls below the threshold at $U_h = 1 - 5$ m s^{-1} (purple-green curves in Fig. 10b). Though cooling is more pronounced in the negative-SSHA features, yet these negative-SSHA features are found in the gyre central region, i.e., a shoaling situation from an existing thick, warm layer (D26~ 80-115m, as in Fig. 2b, and black profiles in Fig. 9a). Therefore, even after shoaling from the negative-SSHA features, the warm layer thickness (in D26) is still around 67-74 m and UOHC around 80 kj cm^{-2} (green profiles in Fig. 9a, Table 4a). Fig. 10b shows that if a storm is fast-moving, i.e. $U_h = 6 - 10$ m s^{-1} (red-brown curves), the self-induced cooling will not exceed the threshold limit since the faster the storm travels, the less pronounced self-induced cooling is induced (Price 1981). Examining the observed translation speed (based on JTWC's best track data) in Table 3, these 3 cases are indeed all relatively fast-traveling storms with U_h between 6.2 and 7.2 m s^{-1}.

In all, it is suggested that two conditions have to be met for storms to reach the category-5 intensity while they are over the negative-SSHA features. First, the negative-SSHA features are over an existing thick enough warm layer, such as over the gyre central region. Second, the storm has to move at a fast enough speed to reduce the negative impact from the self-induced SST cooling. In this work, three real cases of typhoon that reached category 5 while passing the negative SSHA features are demonstrated (cases i, j, k, in Table 3 and Fig. 8).

Interestingly, note that all 3 cases (Ivan, Joan, and Keith, cases i, j, k in Table 3 and Fig. 8) occurred during the El Niño period in October 1997. This suggest that the observed negative-SSHA features are part of the large scale shoaling in the western North Pacific gyre (also see Fig. 1b) because the warm water piled to the Eastern Pacific Ocean during El Niño (Wyrtki 1979; Philander 1990; Johnson et al.

2000).

(2)   Normal (no feature) scenario

As for the cases which do not pass over specific primary features (e.g., Fig. 8f, t), it is understandable that under this no-feature situation, with no deepening or shoaling, the *in situ* profiles (yellow profiles) are very similar to the climatological profiles (black profiles) in Fig. 9b (see also Table 4b). Under this circumstance, the estimated storm-induced SST cooling under both *in situ* (Fig. 10c) and climatological (Fig. 10a) conditions is also similar. From Table 4b, one sees that since the climatological warm layer is already as deep as 117m and UOHC as high as 112 kj cm^{-2}, self-induced cooling can already be well-constrained under the climatological condition (Fig. 10a) that only when U_h = 1 and 2 m s^{-1} would the storm-induced SST cooling exceed the threshold. In Table 3, it is seen that the observed translation speed is 3.0 and 6.4 m s^{-1} for the 2 normal cases (cases f and t), suggesting the self-induced cooling will not exceed the threshold limit at these translation speeds.

(3)   Positive-SSHA features

Followed from above, one can see that in the gyre, the background climatological warm layer is already very deep, with D26 extends to around 108 m and UOHC to 90 kj cm^{-2} (black profiles in Fig. 9c and Table 4c).   Over the positive-SSHA features in the gyre region, the warm layer can extend even deeper, corresponding to D26 of an average of 134m and UOHC of 122 kj cm^{-2} (purple profiles in Fig. 9c and Table 4c). Certainly under this situation, the corresponding storm-induced SST cooling is very limited, only when U_h = 1 and 2 m s^{-1} would the storm-induced SST cooling exceed the threshold limit (Fig. 10d). As shown in Table 3, the observed translation speed of these cases ranges between 2.3 and 9.4 m s^{-1}, confirming that the corresponding self-induced cooling of these storms would not have fallen below the threshold (Fig. 10d).

Comparing the findings in the gyre central and the SEZ, it is found that in the gyre central the background climatological warm layer is already very deep. Therefore the self-induced cooling negative

14

feedback can be suppressed without encountering the positive features. Whereas in the SEZ situation, the background climatological warm layer is much shallower and encountering positive features is critical since the background climatological upper ocean thermal structure could not have supported intensification to category-5.

c. The case in the Kuroshio region

In Fig. 2b, one can see that the background climatological D26 in the Kuroshio region is around 50-80 m (Fig. 2b), roughly in-between the typical values at the SEZ and the gyre region.   In the past 13 years, there is 1 category-5 typhoons peaked in the Kuroshio region and belongs to the positive-SSHA features scenario (Table 5, Fig. 11). In Fig. 11a, we see that typhoon Bart (1999) intensified all the way from category 1 to 5 on a prominent positive-SSHA feature (SSHA ~ 20-40cm) when passing over the Kuroshio region.   Because no *in situ* profile is found in this case, the observed SSHA information is added to a simple 2-layer reduced gravity ocean model[4] (Goni et al. 1996; Shay et al. 2000) to assess the deepening impact of this positive-SSHA feature. The applicability of this model in the western North Pacific has been validated by Pun et al. (2007) using more than 5000 co-incident and co-llocated *in situ* profiles from the ARGO floats (Gould et al. 2004) and the NOAA/GTSPP data base (Keeley et al. 2003). It can be seen that without the positive-SSHA feature, the climatological D26 is between 60 and 80 m (Fig. 11b), while with the positive-SSHA feature, the D26 extends to around 100 m (Fig. 11c), indicating the 30-m deepening (Fig. 11d).

---

[4] At each location (x, y) and time (t), the observed satellite SSHA (η') can be used to estimate the depth of the $20°$ C isotherm (D20 or h_1) as $h_1(x,y,t) = \overline{h_1}(x,y) + \dfrac{\rho_2(x,y)}{\rho_2(x,y) - \rho_1(x,y)} \eta'(x,y,t)$ (eq. 1), where $\overline{h_1}$ is the mean climatological D20 and ρ_1, ρ_2 are the density (calculated from the NOAA/WOA01 temperature and salinity database, Millero et al. 1980; UNESCO 1983) of the 2 layers (i.e., from sea surface to D20 and from D20 the bottom of the ocean). After the D20 estimation, the depth of the $26°$ C isotherm (D26 or H) is estimated based on the climatological ratio (Stephens et al., 2002) between D20 and D26 as: $H(x,y,t) = \theta h_1(x,y,t)$ (eq. 2), where H represents D26 and θ is the climatological ratio. Thus, the difference between the estimated and the climatological D20 and D26 is due to the deepening (or shoaling) by positive (or negative) SSHA features (Goni et al. 1996; Shay et al. 2000).

Without the *in situ* profiles, the storm-induced SST cooling is only estimated using the climatological profiles (black profiles in Fig. 12a). In Fig. 12b, it is shown that because Bart travels very slowly at U_h = 1.9 m s^{-1} (Table 5), it is not possible to support intensification to the fifth category under the climatological condition, as the storm-induced SST cooling could already exceed the threshold of 2.5°C before Bart reaches the fifth category, i.e., at the third and fourth categories. This suggests that passing over the observed positive-SSHA feature is critical to support Bart's intensification to the fifth category, given that the climatological UOTS could not provide the support its intensification to the fifth category

5. Discussion

5.1 Issue on the percentage of category-5 typhoons which require encountering positive-SSHA features during 1993-2005

From section 4, one sees that the situation in the SEZ and Kuroshio region is different from the gyre central situation. In the gyre central region, the background climatological warm layer is already deep enough (D26 ~ 105-117m and UOHC ~ 80-122 kj cm^{-2}) to restrain storm's self-induced ocean cooling, given the observed translation speeds (Table 3). Therefore passing over the positive SSHA features is not critical and storms are observed to intensify to category-5 without encountering any features or even on negative-SSHA features.

However, in the SEZ and the Kuroshio cases, it is critical for these storms to pass over the observed positive-SSHA features because the background climatological warm layer is relatively shallow (D26 ~ 60m and UOHC ~ 50 kj cm^{-2}, Table 2). It is found that given the observed translation speeds (Tables 1 and 5), it is not possible to limit the self-induced cooling negative feedback with the climatological upper ocean thermal structure. As ocean plays a necessary role in intensification (Holliday and Thompson 1979; Emanuel 1986), these cases could not have reached category-5 without keeping the self-induced cooling restrained. In the presence of positive features, the warm layer in this relatively shallow background can

16

be effectively deepened by nearly 100% (D26~ 103m and UOHC ~ 109 kj cm^{-2}, Table 2). This enables the self-induced cooling negative feedback to be limited to support intensification. From Section 4, it can be seen that in the 13 years during 1993-2005, 8 (i.e., 7 SEZ and 1 Kuroshio) out of the 30 category-5 storms belong to this situation. In other words, without encountering the positive-SSHA ocean features, 27% (8/30) of the storms could not have satisfied ocean's part of necessary condition for reaching the category-5 intensity.

Also, it should be clarified that this does not suggest that the other parameters (e.g., atmospheric wind shear and storm structure) are not important in intensification to category-5. Certainly to reach category-5, all related atmospheric, ocean, and storm conditions need to be favorable. The focus of this study is to show whether or not encountering ocean features are required to meet the ocean's part of necessary condition. Because ocean is a necessary condition in intensification, even if all other conditions are met but without meeting one necessary condition, a storm could still not intensify to category-5.

5.2 Issue on the choice of the 2.5°C threshold for self-induced cooling and enthalpy flux

In this work, the 2.5°C threshold proposed by Emanuel (1999) and Emanuel et al. (2004) is adopted to indicate unfavorable condition for intensification. From Emanuel (1999), this amount of cooling is sufficient to shut down the entire energy production of a storm. To further substantiate this, we calculate the corresponding air-sea sensible (Q_S) and latent heat fluxes (Q_L) using the bulk aerodynamic formulae (Jacob et al. 2000; Cione and Uhlhorn 2003; Powell et al. 2003; Black et al. 2007) as follows:

$Q_S = C_H W (T_s - T_a)\rho_a C_{pa}$ (2) and $Q_L = C_E W (q_s - q_a)\rho_a L_{va}$ (3), where C_H and C_E are the sensible and the latent heat (moisture) exchange coefficients, W is the wind speed, T_s and T_a represent SST and near surface air temperature, q_s and q_a represent surface and air specific humidity, ρ_a, C_{pa}, and L_{va} are air density, heat capacity of the air, and latent heat of vaporization. In this work, the exchange coefficients are from Black et al. (2007), wind speed is form JTWC's best track data, the near surface atmospheric data is from the 1.125° resolution data (ERA 40) of the ECMWF (European Center for

17

Medium Range Weather Forecast), and the SST data is from the output of the mixed layer model, i.e., with incorporation of the self-induced cooling effect.

As the flux calculation requires multiple input data sets (e.g., ECMWF atmospheric data and *in situ* UOTS profiles for the mixed layer model), we were able to calculate the sensible and latent heat fluxes for 7 cases during 2001-2005. Among them, 2 cases belong to the SEZ/Positive-SSHA feature scenario (i.e., Maemi (2003) and Maon (2004)), 1 case belongs to the gyre/normal scenario (i.e., Chaba (2004)), and 4 cases belong to the gyre/positive-SSHA feature scenario (i.e., Hagibis (2002), Fengshen (2002), Dianmu (2004), and Nabi (2005)). For each case, sensible and latent heat fluxes are estimated under the *in situ* (i.e., with feature) and the climatological condition.

Fig. 13 depicts the average available enthalpy (sensible + latent heat fluxes) under the different conditions. It can be seen that the flux condition also suggests that under the SEZ_climatological condition (blue curve), there won't be sufficient energy to support intensification to category-5. As in Fig. 13, the average enthalpy reaches zero at category-3 and 4, showing unfavorable condition for continual intensification to category-5. However, if encountering positive-SSHA feature in the SEZ (i.e., yellow curve), the available enthalpy supply increases significantly. One can see that available enthalpy increases during the intensification process (e.g., more than 1000W m^{-2} is available at category-4), showing favorable condition for continual intensification to category-5.

The flux situation in the gyre central also concurs with the findings in Section 4 that in the gyre central region, even without encountering positive-SSHA features, the background climatology can also provide sufficient energy for intensification. One can see in Fig. 13 that the available enthalpy condition is around 1000 W m^{-2} at category-3 and around 1300 W m^{-2} at category-4 for the gyre_climatology (blue curve) and the gyre_neutral (i.e., green curve) conditions.

5.3 Issue on 1-D .vs. 3-D ocean simulations

Finally, as the 1-D mixed layer model (Price et al. 1986) is a simple ocean model and does not account for the possible lateral transport associated with the ocean eddies (Jacob et al. 2000; Jacob and

Shay 2003), a full 3-D ocean model is used to assess the possible difference. The model used is the EASNFS model from the US Naval Research Lab (Ko et al. 2003; Chapman et al. 2004). It is an experimental real-time Ocean Nowcast/Forecast System for the East Asian Seas. The model domain covers 17.3°S to 52.2°N and 99.2°E to 158.2°E. The system produces nowcast for the sea level variation, 3-D ocean current, temperature and salinity fields. EASNFS is a 41-level sigma-z data-assimilating ocean model and the spatial resolution is 1/16 degree. Real-time satellite altimetry sea surface height anomaly data (e.g., TOPEX/Poseidon and JASON-1) and SST (e.g., NOAA/AVHRR) are assimilated to produce realistic nowcast of the ocean condition in the western North Pacific. Three hourly surface heat fluxes, solar radiation, wind stresses and sea level air pressure from NRL's NOGAPS system are used for surface forcing.

In this work, the 3-D simulation is performed on the case of supertyphoon Maemi (2003) (Lin et al. 2005) as the ocean eddy associated with this case is the largest in the eddy rich zone (i.e., SEZ, see Fig. 5f). In the simulations, 2 experiments are run, one is the full simulation (i.e., including both 1-D mixing and lateral effects) and the other is the no-mixing run (i.e., switching off the 1-D mixing component). Fig. 14 depicts the simulation results for 3 locations where Points b and c represent the 'inside eddy' condition and Point a represent the 'outside eddy' condition (Fig. 14d). From Figs. 14 b and c, one can see that in the no-mixing runs (blue curves), there is little difference before and after typhoon's passing. Only with the inclusion of the 1-D mixing effect (pink curves) can the cooling effect induced by typhoon's forcing be seen. As in Fig. 14a, similar situation is found in the outside region. These results support previous reports that the 1-D mixing effect is the primary mechanism in cyclone's self-induced cooling and it is applicable to use the 1-D mixed layer model to assess the self-induced cooling in this work (Price 1981; Gallacher et al. 1989; Emanuel 1999; Jacob et al. 2000; Jacob and Shay 2003; Emanuel et al. 2004).

6. Conclusions

There is much interest to study the role ocean features play in the intensification of category-5 typhoons. Based on the *in situ* upper ocean thermal structure profiles, satellite altimetry and the SST

data, JTWC's best-track typhoon data, climatological ocean thermal structure data, and an ocean mixed layer model, this work systematically studies the role ocean features play in the 30 western North Pacific category-5 typhoons occurring during the May-October typhoon season in 1993-2005.

It is found that the background climatological upper ocean thermal structure is an important factor in determining the criticalness of feature-encountering. If the background climatological warm layer is already deep enough, for example in the gyre central region where D26~110m and UOHC ~ 100 kj cm^{-2}, then passing over the positive SSHA features is not critical because the background itself can already effectively restrain the negative feedback to intensity from cyclone's self-induced ocean cooling. In the gyre central region, typhoons are found to intensify to category-5 not only over positive SSHA features, but also without encountering features, or even when passing over negative SSHA features.

However, in the relatively shallow background, for example in the SEZ and the Kuroshio regions where D26 ~ 60m and UOHC ~ 50 kj cm^{-2}, passing over positive SSHA features is critical in order to meet the ocean's part of necessary condition in intensification. It is found that without the deepening of warm layer by the features, it is not possible to restrain the self-induced cooling negative feedback to support intensification as there won't be sufficient sensible and latent heat fluxes available. In the past 13 years, all 8 cases passed through these 2 regions belong to this situation.

Finally, it should be clarified that certainly to reach the category-5 intensity, a full suite of necessary conditions (e.g., atmospheric vertical wind shear and storm structure conditions) all need to be met (Gray 1979; Holliday and Thompson 1979; Emanuel et al. 2004; Houze et al. 2007). The focus of this work is to discuss whether it is critical to encounter ocean features to meet the ocean's part of necessary condition in intensification. It does not imply that other necessary conditions are not important in intensification. Followed from this work, in the Part II of the series, issues regarding ocean's thermal structure with cyclone's translation speed and geographical dependence for the western North Pacific category-5 typhoons will be addressed.

References

Bender, M. A., and I. Ginis, 2000: Real-case simulations of hurricane-ocean interaction using a high-resolution coupled model: effects on hurricane intensity. *Mon. Wea. Rev.,* 128, 917-946.

Black, P. G., E. A. D'Asaro, W. M. Drenna, J. R. French, P. P. Niiler, T. B. Sanford, E. J. Terrill, E. J. Walsh, and J. A. Zhang, 2007: Air—Sea Exchange in Hurricanes, *Bull. Amer. Meteor. Soc.,* 88 (3), 357-374.

Chapman, D. C., D. S. Ko, and R. H. Preller, 2004: A High-Resolution Numerical Modeling Study of the Subtidal Circulation in the Northern South China Sea. *IEEE J. Oceanic Engineering*, 29(4), 1087-1104.

Cione, J. J., and E. W. Uhlhorn, 2003: Sea surface temperature variability in hurricanes: Implications with respect to intensity change. *Mon. Wea. Rev.,* 131, 1783-1796.

Emanuel, K. A., 1986: An air-sea interaction theory for tropical cyclones Part I. *J. Atmos. Sci.*, 42, 1062–1071.

Emanuel, K. A., 1999: Thermodynamic control of hurricane intensity. *Nature,* 401, 665-669.

Emanuel, K. A., 2000: A statistical analysis of tropical cyclone intensity. *Mon. Wea. Rev.,* 128, 1139-1152.

Emanuel, K. A., C. DesAutels, C. Holloway, and R. Korty, 2004: Environmental control of tropical cyclone intensity. *J. Atmos. Sci.,* 61, 843–858.

Emanuel, K. A., 2006: Climate and tropical cyclone activity: A new model downscaling approach. *J. Climate*, 19, 4797-4802.

Fu, L. L., E. J. Christensen, C. A. Yamarone, M. Lefebvre, Y. Menard, M. Dorrer, and P. Escudier, 1994: TOPEX/POSEIDON Mission Overview. *J. Geophys. Res.,* 99, 24369-24381.

Gallacher, P. C., R. Rotunno, and K. A. Emanuel, 1989: Tropical cyclogenesis in a coupled ocean–atmosphere model. Preprints, *18th Conf. on Hurricanes and Tropical Meteorology*, San Diego, CA, Amer. Meteor. Soc., 121–122.

Goni, G. J., S. Kamholtz, S. Garzoli, and D. B. Olson, 1996: Dynamics of the Brazil–Malvinas confluence based upon inverted echo sounders and altimetry. *J. Geophys. Res.,* 101 (7), 16273–16289.

Goni, G. J., and J. A. Trinanes, 2003: Ocean thermal structure monitoring could aid in the intensity forecast of tropical cyclones. *EOS, Trans. Amer. Geophys. Union,* 84, 573-580.

Gould, J., D. Roemmich, S. Wijffels, H. Freeland, M. Ignaszewesky, X. Jianping, S. Pouliquen, Y. Desaubies, U. Send, K. Radhakrishnan, K. Takeuchi, K. Kim, M. Danchenkov, P. Sutton, B. King, B. Owens, and S. Riser, 2004: Argo Profiling Floats Bring New Era of In Situ Ocean Observations. *EOS, Trans. Amer. Geophys. Union,* 85, 179&190-191.

Gray, W. M., 1979: Hurricanes: Their formation, structure and likely role in the tropical circulation. *Meteorology over the Tropical Oceans,* D. B. Shaw, Ed., Royal Meteorological Society, 155–218.

Holliday, C. R., and A. H. Thompson, 1979: Climatological characteristics of rapidly intensifying typhoons. *Mon. Wea. Rev.*, 107, 1022-1034.

Houze Jr., R. A., S. S. Chen, B. F. Smull, W. C. Lee, and M. M. Bell, 2007: Hurricane intensity and eyewall replacement, *Science*, 315, 1235–1239.

Hwang, C., C. R. Wu, and R. Kao, 2004: TOPEX/Poseidon observations of mesoscale eddies over the subtropical countercurrent: kinematic characteristics of an anticyclonic eddy and of a cyclonic eddy. *J. Geophy. Res.*, 109, C08013, doi:10.1029/2003JC002026.

Jacob, S. D., L. K. Shay, A. J. Mariano, and P. G. Black, 2000: The 3D oceanic mixed layer response to hurricane Gilbert. *J. Phys. Oceanogr.,* 30, 1407-1429.

Jacob, S. D., and L. K. Shay, 2003: The role of oceanic mesoscale features on the tropical-cyclone induced mixed layer response. *J. Phys. Oceanogr.*, 33, 649-676.

Johnson, G. C., M. J. McPhaden, G. D. Rowe, and K. E. McTaggert, 2000: Upper equatorial Pacific Ocean current and salinity variability during the 1996—1998 El Niño-La Niña cycle. *J. Geophys. Res.*, 105, 1037—1053.

Kaplan, J., and M. DeMaria, 2003: Large-scale characteristics of rapidly intensifying tropical cyclones in the North Atlantic basin. *Wea. Forecasting*, 18, 1093-1108.

Keeley, B., C. Sun, and L. P. Villeon, 2003: Global Temperature and Salinity Profile Program Annual Report. NOAA/National Oceanographic Data Center, Silver Spring, MD.

Ko, D. S., R. H. Preller, G. A. Jacobs, T. Y. Tang, and S. F. Lin, 2003: Transport reversals at Taiwan Strait during October and November 1999. *J. Geophys. Res.*, 108, C11, 3370.

Leipper, D., and D. Volgenau, 1972: Hurricane heat potential of the Gulf of Mexico. *J. Phys. Oceanogr.,* **2**, 218-224.

Lin, I I, W. T. Liu, C. C. Wu, J. C. H. Chiang, and C. H. Sui, 2003a: Satellite observations of modulation of surface winds by typhoon-induced upper ocean cooling. *Geophys. Res. Lett.,* **30**, 1131, doi:10.1029/2002GL015674.

Lin, I I, W. T. Liu, C. C. Wu, G. T. F. Wong, C. Hu, Z. Chen, W. D. Liang, Y. Yang, and K. K. Liu, 2003b: New evidence for enhanced ocean primary production triggered by tropical cyclone. *Geophys. Res. Lett.,* **30**, 1718, doi:10.1029/2003GL017141.

Lin, I I, C. C. Wu, K. A. Emanuel, I. H. Lee, C. R. Wu, and I. F. Pun, 2005: The Interaction of Supertyphoon Maemi (2003) With a Warm Ocean Eddy. *Mon. Wea. Rev.,* 133, 2635-2649.

Liu, K. S., and J. C. L. Chan, 1999: Size of tropical cyclones as inferred from ERS−1 and ERS−2 data. *Mon. Wea. Rev.*, 127, 2992−3001.

Merrill, R. T., 1984: Structure of the tropical cyclone outflow layer. *Proc. 15th Conf. on Hurricanes and Tropical Meteorology,* Miami, FL, Amer. Meteor. Soc., 421–426.

Millero, F. J., C. T. Chen, A. Bradshaw, and K. Schleicher, 1980: A new high pressure equation of state for seawater. *Deep Sea Res.*, 27A, 255-264.

Oey, L.Y., T. Ezer, D.-P. Wang, S.-J. Fan and X.-Q. Yin, Loop Current warming by Hurricane Wilma, *Geophys. Res. Lett.*, 33, L08613, doi:10.1029/2006GL025873, 2006

Philander, S. G. H., 1990: *El Niño, La Niña, Southern Oscillation. Academic Press*, 293 pp.

Pickard, G. L., and W. J. Emery, 1990: Descriptive physical oceanography, *Pregamon Press*.

Powell, M. D., P. J. Vickery, and T. A. Reinhold, 2003: Reduced drag coefficient for high wind speeds in tropical cyclones. *Nature*, 422, 279-283.

Price, J. F., 1981: Upper ocean response to a hurricane. *J. Phys. Oceanogr.,* 11, 153–175.

Price, J. F., R. A. Weller, and R. Pinkel, 1986: Diurnal cycling: Observations and models of the upper

ocean response to diurnal heating, cooling, and wind mixing. *J. Geophys. Res.*, 91, 8411-8427.

Pun, I. F., I. I. Lin, C. R. Wu, D. S. Ko, and W. T. Liu, 2007: Validation and Application of Altimetry-derived Upper Ocean Thermal Structure in the Western North Pacific Ocean for Typhoon Intensity Forecast. *IEEE Trans. Geosci. Remote Sens.* 45(6), 1616-1630.

Qiu, B., 1999: Seasonal eddy field modulation of the North Pacific Subtropical Countercurrent: TOPEX/Poseidon observations and theory. *J. Phys. Oceanogr.* , 29, 1670-1685.

Richard H.B., 1981: Gulf stream cold-core rings: their physics, chemistry, and biology. *Science*, 212, 1091-1100.

Roemmich, D., and J. Gilson, 2001: Eddy transport of heat and thermocline waters in the north pacific: a key to interannual/decadal climate variability? *J. Phys. Oceanogr.*, 13, 675-687.

Scharroo, R., W. H. F. Smith, and J. L. Lillibridge, 2005: Satellite Altimetry and the Intensification of Hurricane Katrina. *EOS, Trans. Amer. Geophys. Union*, 86, 366-367.

Shay, L. K., G. J. Goni, and P. G. Black, 2000: Effects of a warm oceanic feature on Hurricane Opal. *Mon. Wea. Rev.*, 128, 1366-1383.

Stephens, C., Antonov, J. I., Boyer T. P., Conkright M. E., Locarnini R. A., O'Brien TD, Garcia HE. 2002: World Ocean Atlas 2001 Volume 1: Temperature, S. Levitus, Ed., NOAA Atlas NESDIS 49. *U. S. Government Printing Office*: Washington, D. C.

UNESCO 1983: Algorithms for computation of fundamental properties of seawater. *Unesco Tech. Pap. in Mar. Sci.* 44, 53.

Wada, A., and N. Usui, 2007: Importance of Tropical Cyclone Heat Potential for Tropical Cyclone Intensity and Intensification in the Western North Pacific, *J. Oceanogr.*, 63, 427-447.

Wang, Y., and C. C. Wu, 2003: Current understanding of tropical cyclone structure and intensity changes - A review. *Meteor. Atmos. Phys.*, 87, 257-278, DOI: 10.1007/s00703-003-0055-6.

Wentz F. J., C. Gentemann, D. Smith, D. Chelton, 2000: Satellite measurements of sea surface temperature through clouds. *Science*, 288, 5467, 847-850.

Wu, C. C., C. Y. Lee, and I. I. Lin, 2007: The Effect of the Ocean Eddy on Tropical Cyclone Intensity. *J.*

Atmos. Sci., 64, 3562-3578.

Wyrtki, K., 1979: The response of sea surface topography to the 1976 El Niño. *J. Phys. Oceanogr.,* **9,** 1223–1231.

Yasuda, I., K. Okuda, and M. Hirai, 1992: Evolution of a Kuroshio warm-core ring – variability of the hydrographic structure. *Deep-Sea Res*., 39, 131-161.

Acknowledgements

Table captions:

Table 1: The 7 SEZ cases and the primary features encountered during intensification.　Intensification period and the average translation speed (U_h) when passing over features are also summarized.

Table 2: Comparison of D26, UOHC, and SST between *in situ* profiles in the positive-SSHA features and the background climatology.

Table 3: The 22 gyre cases and the primary features encountered during intensification. Intensification period and the average translation speed (U_h) when passing over features are also summarized.

Table 4: Comparison of D26, UOHC, and SST between *in situ* profiles and the background climatology in the gyre for (a) negative-SSHA feature scenario, (b) normal (no feature scenario), and (c) positive-SSHA feature scenario.

Table 5: The Kuroshio case and the primary feature encountered during intensification.　Intensification period and the average translation speed (U_h) when passing over the feature are also summarized.

Figure captions:

Fig. 1: Exemplary monthly-averaged SSHA (in cm) maps (a: June 2004, b: October 1997) from the TOPEX/Poseidon and JASON-1 satellite altimeters (tracks depicted in yellow) showing abundant positive (shaded in red) and negative (shaded in blue) SSHA features are present in the western North Pacific Ocean. The locations of the North Eddy Zone (NEZ), South Eddy Zone (SEZ), Kuroshio, gyre, and the South China Sea (SCS) are depicted. Mesoscale features are often found in the North Eddy Zone (NEZ) and the South Eddy Zone (SEZ); while large, basin scale features are often found in the gyre.

Fig. 2: The background climatological upper ocean thermal structure (in SST and D26) during the western North Pacific summer (July-September). (a) SST, as observed by the TRMM satellite during 2000-2005. (b) D26, data from the 0.25° resolution monthly climatological data of the

NOAA/World Ocean Atlas 2001 (Stephens et al. 2002).

Fig. 3: Schematic diagram showing the situation as typhoon approaches a point location in ocean, as simulated by the 1-D mixed layer model. The inner core diameter (D) used in this work is 220km and the TC_transit time is calculated as D/Uh.

Fig. 4: Full tracks (in grey) and the intensification (from category 1 to 5) track segment (in red) of the 30 category-5 typhoons occurred during May-October between 1993 and 2005. Locations of the *in situ* profiles are depicted as stars.

Fig. 5: Pre-typhoon SSHA (in cm) maps and the tracks of the 7 SEZ cases (in chronological order, see also Table 1). Locations of the *in situ* profiles are depicted as green stars. The altimetry tracks are depicted in yellow.

Fig. 6: *In situ* depth-temperature profiles (in red) found in the positive-SSHA features in the SEZ (location depicted as green stars in Fig. 5). For comparison, the background climatological profiles along the track of the 7 SEZ cases are also depicted (black profiles).

Fig. 7: Estimation of typhoon's self-induced ocean cooling using the Price-Weller-Pinkel ocean mixed layer model (Price et al. 1986) for the SEZ cases. The storm-induced cooling is estimated progressively with increase in wind forcing (every 5 m s^{-1} interval) from category-1 to 5 (denoted as C1-C5) at various translation speeds (U_h= 1,2,3,…10 m s^{-1}). Region of self-induced cooling exceeding the 2.5°C threshold (from Emanuel 1999) is shaded in grey, indicating unsuitable condition for intensification. (a) Estimation based on the climatological profiles (black profiles) along the typhoon tracks. (b) Estimation based on the *in situ* profiles (red profiles in Fig. 6) inside the positive-SSHA features.

Fig. 8: Pre-typhoon SSHA (in cm) maps and the tracks of the 22 SEZ cases (in chronological order, see also Table 3). Locations of the *in situ* profiles are depicted as green stars. The altimetry tracks are depicted in yellow.

Fig. 9: *In situ* depth-temperature profiles (in color) .vs. the background climatological profiles (in black)

for various scenarios in the gyre. (a) The negative-SSHA feature scenario. (b) The normal (no feature) scenario. (c) The positive-SSHA feature scenario. Locations of the *in situ* profiles are depicted as green stars in Fig. 8.

Fig. 10: As in Fig. 7, but for the self-induced ocean cooling estimation for the gyre cases. (a) Estimation based on the climatological profiles (black profiles) along the typhoon tracks. (b) Estimation based on the *in situ* profiles (green profiles in Fig. 9a) inside the negative-SSHA features. (c) Estimation based on the *in situ* profiles (yellow profiles in Fig. 9b) under normal (no feature) condition. (d) Estimation based on the *in situ* profiles (purple profiles in Fig. 9c) inside the positive-SSHA features.

Fig. 11: The Kuroshio – positive SSHA feature case (i.e. Bart (1999), see also Table 3). (a) Pre-typhoon SSHA (in cm) map and the TC track. The altimetry tracks are depicted in yellow. (b) The background climatological D26 from the NOAA/World Ocean Atlas 2001 (Stephens et al. 2002). (c) The positive-feature modulated D26, as estimated from a 2-layer reduced gravity ocean model proposed by Goni et al. (1996) and Shay et al. (2000). (d) The deepening of D26 by the positive SSHA feature (i.e., (c)) as compared with climatology (i.e., (b)).

Fig. 12: (a) Climatological depth-temperature profiles along the track of typhoon Bart (1999). (b) As in Fig. 7, but for the self-induced ocean cooling estimation using the climatological profiles in (a).

Fig. 13: The estimated available enthalpy (sensible + latent heat flux) during various stages of intensification for different scenarios: gyre climatology (blue dashed curve), gyre positive (red curve), gyre neutral (green curve), SEZ climatology (light-blue dashed curve), and SEZ positive (yellow curve).

Fig. 14: 3-D numerical experiments using the US NRL's EASNFS ocean model showing upper ocean temperature evolution (average from surface to 20m depth) before, during, and after typhoon's passing for 3 locations. As shown in (d), Points b and c are located in the warm eddy while point a locates at the outside of the eddy. For each point, simulation is done with mixing (pink curves) and without mixing (blue curves).

Table 1: The 7 SEZ cases and the primary features encountered during intensification. Intensification period and the average translation speed (U_h) when passing over features are also summarized.

Typhoon	Year/Month	Intensification Period	Primary Feature	Altimetry cycle	*Uh (m/s)*
a. 95_17	1995/09	0914/00Z-0915/06Z	+	0903-0912	5.3
b. Eve	1996/07	0715/00Z-0716/00Z	+	0704-0713	5.2
c. Herb	1996/07	0726/00Z-0730/18Z	+	0716-0725	4.5
d. Ginger	1997/09	0926/00Z-0927/00Z	+	0916-0925	3.7
e. Saomai	2000/09	0908/12Z-0910/12Z	+	0828-0906	5.2
f. Maemi	2003/09	0908/18Z-0910/00Z	+	0828-0906	4.8
g. Maon	2004/10	1007/00Z-1008/00Z	+	0925-1004	3.0

Table 2: Comparison of D26, UOHC, and SST between *in situ* profiles in the positive-SSHA features and the background climatology.

Table 2 SEZ/ +SSHA feature	*In situ* profiles	*In situ* D26 (m)	D26 (m) (Climatology)	ΔD26 (m)	*In situ* UOHC (kj cm⁻²)	UOHC (climat.) (kj cm⁻²)	ΔUOHC (kj cm⁻²)	*In situ* SST (°C)	SST (°C) (Climatology)	ΔSST (°C)
	Saomai (2000)	90	58	+32	73	44	+29	28.2	28.5	-0.3
	Maemi_1	114	63	+51	133	52	+81	29.3	28.7	+0.6
	Maemi_2	95	63	+32	119	51	+68	29.6	28.7	+0.9
	Maon	111	63	+48	109	40	+69	29.0	27.9	+1.1
	Average	**103**	**62**	**+41**	**109**	**47**	**+62**	**29**	**28.5**	**+0.5**

Table 3: The 22 gyre cases and the primary features encountered during intensification. Intensification period and the average translation speed (U_h) when passing over features are also summarized.

Typhoon	Year_Month	Intensification Period	Primary Feature	TP/J cycle	Uh (m/s)
a. 93_25	1993_10	1002/00Z-1004/12Z	+	0921-0930	4.8
b. 94_17	1994_08	0804/00Z-0805/18Z	+	0723-0801	5.3
c. 95_26	1995_10	1018/00Z-1019/12Z	+	1006-1015	8.2
d. 95_29	1995_10	1030/06Z-1101/00Z	+	1017-1026	4.3
e. Sally	1996_09	0906/12Z-0907/18Z	+	0824-0904	8.8
f. Nestor	1997_06	0608/18Z-0610/12Z	Normal	0528-0606	3.0
g. Rosie	1997_07	0721/06Z-0722/12Z	+	0710-0719	3.0
h. Winnie	1997_08	0810/06Z-0812/00Z	+	0730-0808	5.0
i. Ivan	1997_10	1015/18Z-1017/18Z	-	1004-1013	7.2
j. Joan	1997_10	1015/18Z-1017/06Z	-	1004-1013	6.7
k. Keith	1997_10	1030/12Z-1101/12Z	-	1010-1028	6.2
l. Zeb	1998_10	1011/18Z-1013/12Z	+	0930-1009	7.0
m. Damrey.	2000_05	0508/06Z-0509/18Z	+	0425-0505	3.7
n. Bilis	2000_08	0820/06Z-0821/18Z	+	0808-0817	6.0
o. Podul	2001_10	1022/06Z-1024/06Z	+	1011-1020	2.3
p. Hagibis	2002_05	0518/12Z-0519/12Z	+	0506-0515	3.6
q.Fengshen	2002_07	0715/00Z-0721/12Z	+	0704-0713	2.7
r. Nida	2004_05	0515/00Z-0516/12Z	+	0504-0513	4.5
s. Dianmu	2004_06	0615/00Z-0616/06Z	+	0603-0612	3.6
t. Chaba	2004_08	0821/12Z-0823/00Z	Normal	0809-0818	6.4
u. Haitang	2005_07	0714/06Z- 0716/12Z	+	0702-0711	9.4
v. Nabi	2005_08	0830/18Z-0901/18Z	+	0819-0828	5.0

Negative-SSHA cases: i, j, k, observed range of *Uh:* 6.2-7.2 m s^{-1}

Normal cases: f, t; observed range of *Uh:* 3.0-6.4 m s^{-1}

Positive-SSHA cases: a-e, g, h, l-s, u, v; observed range of *Uh:* 2.3-9.4m s^{-1}

Table 4: Comparison of D26, UOHC, and SST between *in situ* profiles and the background climatology in the gyre for (a) negative-SSHA feature scenario, (b) normal (no feature scenario), and (c) positive-SSHA feature scenario.

Table 4a gyre/ - SSHA feature	*In situ* profiles	*In situ* D26 (m)	D26 (m) (Climatology)	Δ D26 (m)	*In situ* UOHC (kj cm^{-2})	UOHC (climat.) (kj cm^{-2})	ΔUOHC (kj cm^{-2})	*In situ* SST (°C)	SST (°C) (Climatology)	Δ SST (°C)
	Joan_1	74	105	-31	82	101	-19	29.8	29.1	+0.7
	Joan_2	67	105	-38	77	104	-27	29.7	29.1	+0.6
	Average	**71**	**105**	**-35**	**80**	**103**	**-23**	**29.8**	**29.1**	**+0.7**

Table 4b gyre/ normal	*In situ* profiles	*In situ* D26 (m)	D26 (m) (Climatology)	Δ D26 (m)	*In situ* UOHC (kj cm^{-2})	UOHC (climat.) (kj cm^{-2})	ΔUOHC (kj cm^{-2})	*In situ* SST (C)	SST (°C) (Climatology)	Δ SST (°C)
	Chaba	121	116	+5	116	118	-2	29.4	29.3	+0.1
	Nestor	113	118	-5	115	105	+10	29.1	29.1	0.
	Average	**117**	**117**	**0**	**116**	**112**	**+4**	**29.3**	**29.2**	**+0.1**

Table 4c gyre/ +SSHA feature	*In situ* profiles	*In situ* D26 (m)	D26 (m) (Climatology)	Δ D26 (m)	*In situ* UOHC (kj cm^{-2})	UOHC (climat.) (kj cm^{-2})	ΔUOHC (kj cm^{-2})	*In situ* SST (°C)	SST (°C) (Climatology)	Δ SST (°C)
	Bilis	114	90	+24	122	83(L2)	+39	29.8	29.2	+0.6
	Hagibis_1	141	106	+37	114	70(L1)	+44	28.8	28.7	+0.1
	Hagibis_2	153	106	+49	131	70(L1)	+61	28.6	28.7	-0.1
	Fengshen_1	125	97	+27	105	80(L4)	+25	29.3	29.0	+0.3
	Fengshen_2	129	97	+31	104	80(L4)	+24	28.8	29.0	-0.2
	Dianmu_1	149	122	+35	144	110(L4)	+34	29.7	29.1	+0.6
	Dianmu_2	128	122	+14	128	110(L4)	+18	29.5	29.1	+0.4
	Nabi	134	120	+19	129	116(L1)	+13	29.7	29.4	+0.4
	Average	**134**	**108**	**+29**	**122**	**90**	**+32**	**29.3**	**29.0**	**+0.3**

Table 5: The Kuroshio case and the primary feature encountered during intensification. Intensification period and the average translation speed (U_h) when passing over the feature are also summarized. .

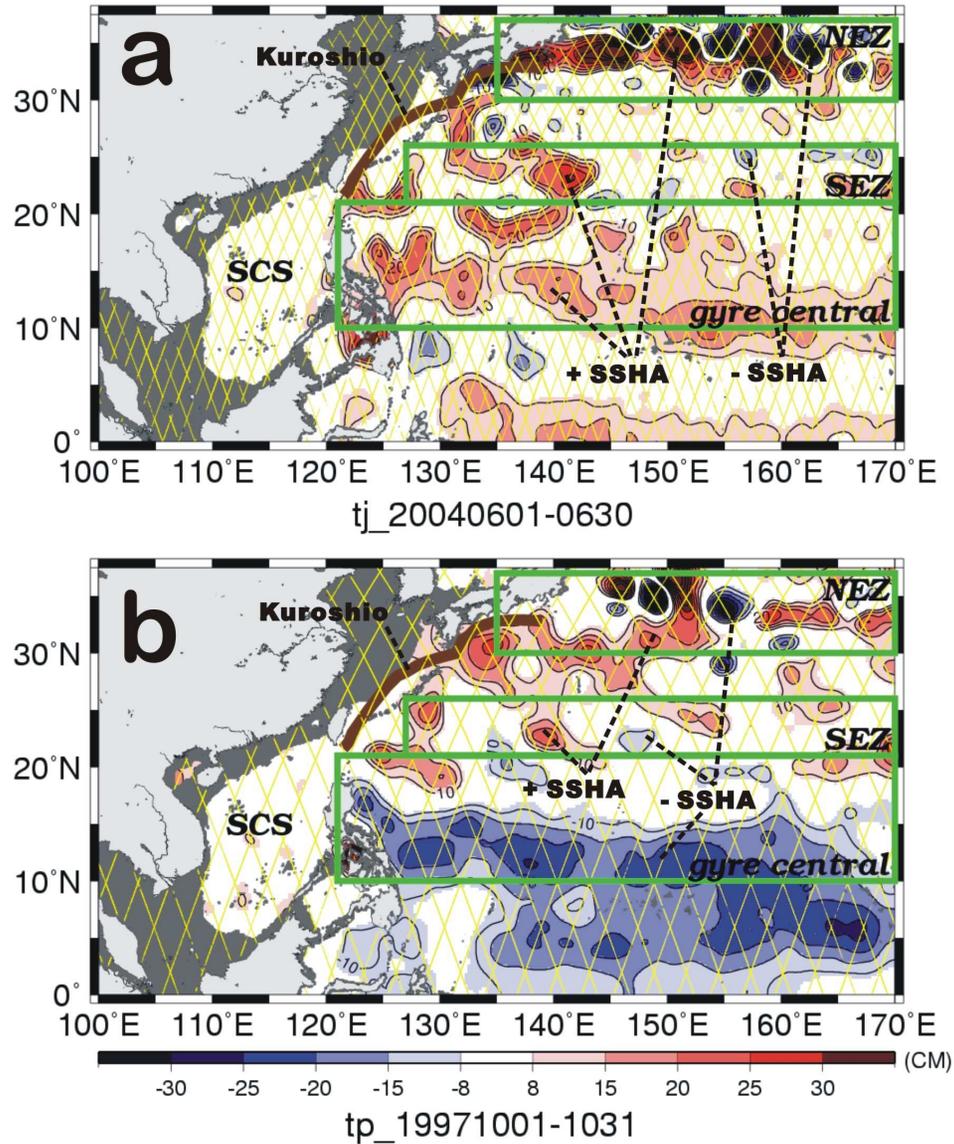| Typhoon	Year_Month	Intensification Period	Primary Feature	TP/J cycle date	*Uh*
a. Bart	1999_09	0920/12Z-0922/06Z	+	0909-0918	1.9

Fig. 1: Exemplary monthly-averaged SSHA (in cm) maps (a: June 2004, b: October 1997) from the TOPEX/Poseidon and JASON-1 satellite altimeters (tracks depicted in yellow) showing abundant positive (shaded in red) and negative (shaded in blue) SSHA features are present in the western North Pacific Ocean. The locations of the North Eddy Zone (NEZ), South Eddy Zone (SEZ), Kuroshio, gyre, and the South China Sea (SCS) are depicted. Mesoscale features are often found in the North Eddy Zone (NEZ) and the South Eddy Zone (SEZ); while large, basin scale features are often found in the gyre central.

Fig. 2: The background climatological upper ocean thermal structure (in SST and D26) during the western North Pacific summer (July-September). (a) SST, as observed by the TRMM satellite during 2000-2005. (b) D26, data from the 0.25° resolution monthly climatological data of the NOAA/World Ocean Atlas (Stephens et al. 2002).
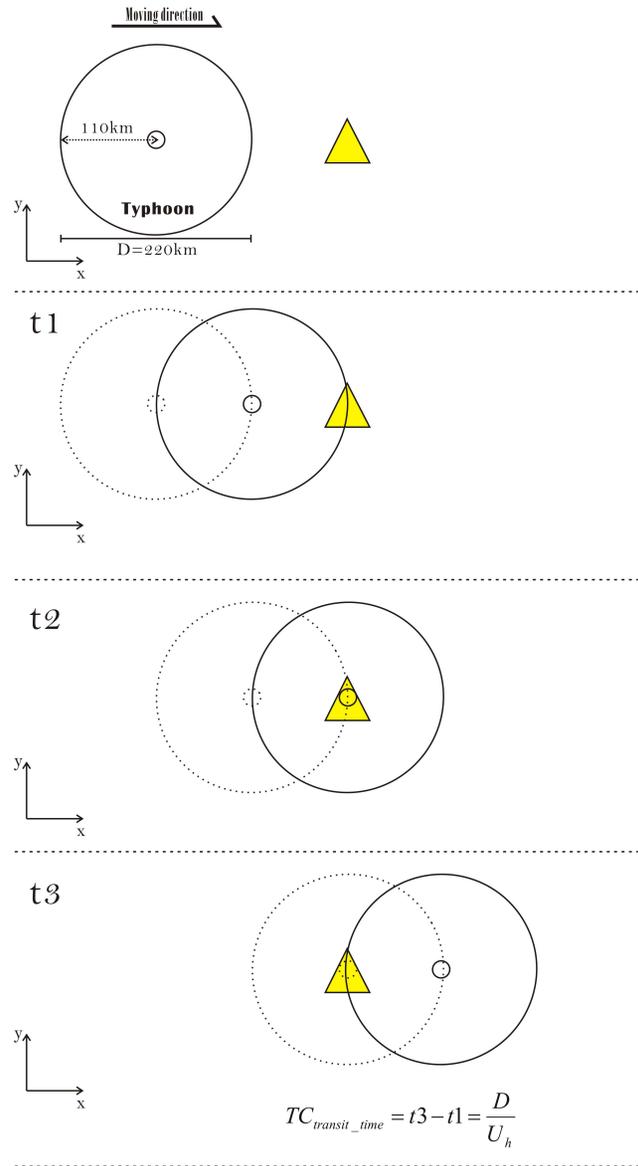
Fig. 3: Schematic diagram illustrating the situation as typhoon approaches a point location in ocean, as simulated by the 1-D mixed layer model. The inner core diameter (D) used in this work is 220km and the TC_transit time is calculated as D/Uh.

Fig. 4: Full tracks (in grey) and the intensification (from category 1 to 5) track segment (in red) of the 30 category-5 typhoons occurred during May-October between 1993 and 2005. Locations of the *in situ* profiles are depicted as stars.
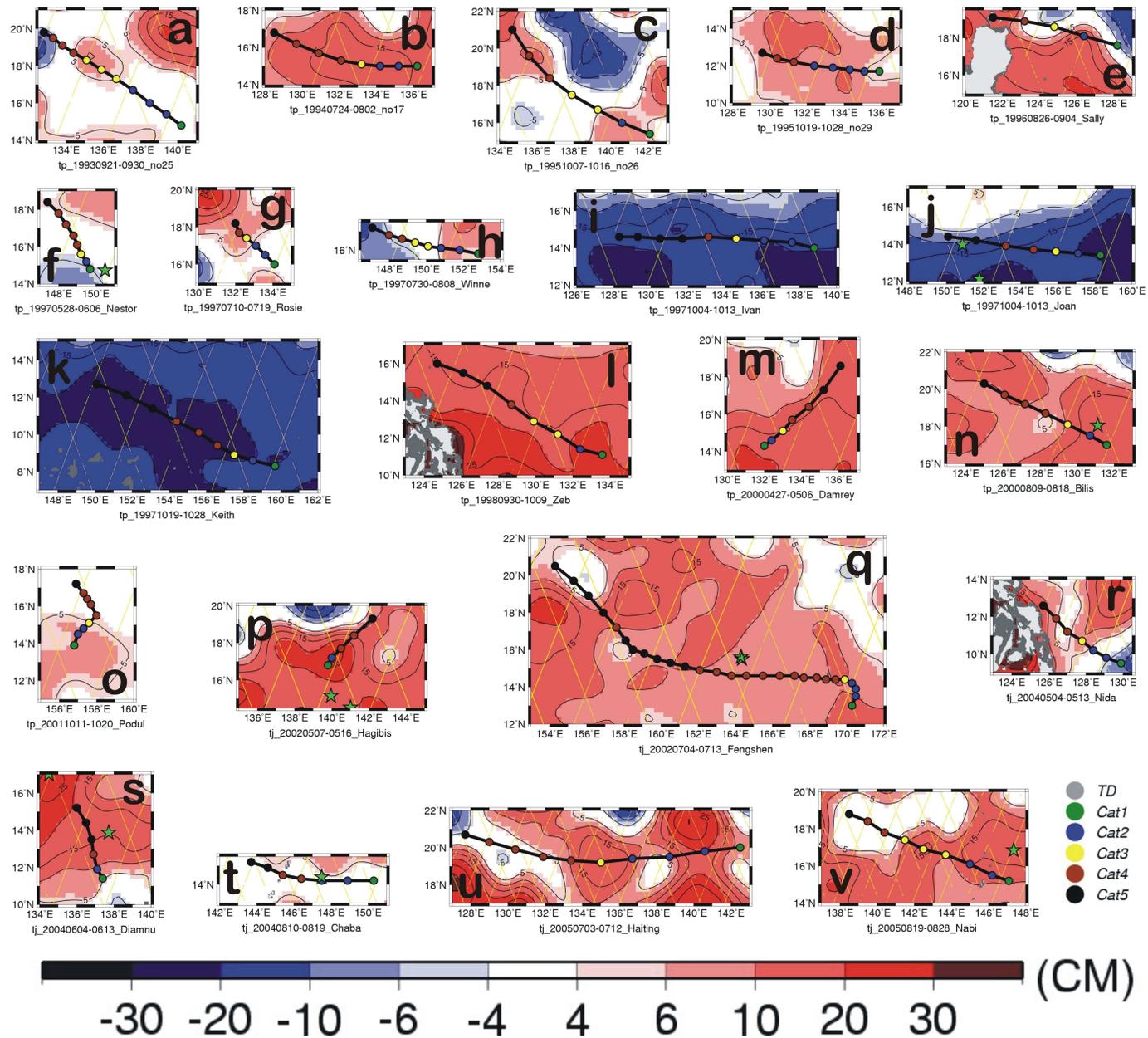
Fig. 5: Pre-typhoon SSHA (in cm) maps and the tracks of the 7 SEZ cases (in chronological order, see also Table 1). Locations of the *in situ* profiles are depicted as green stars. The altimetry tracks are depicted in yellow.

Fig. 6: *In situ* depth-temperature profiles (in red) found in the positive SSHA features in the SEZ (location depicted as green stars in Fig. 4). For comparison, the background climatological profiles along the track of the 7 SEZ cases are also depicted (black profiles).

Fig. 7: Estimation of typhoon's self-induced ocean cooling using the Price-Weller-Pinkel ocean mixed layer model (Price et al. 1986) for the SEZ cases. The storm-induced cooling is estimated progressively with increase in wind forcing (every 5 m s-1 interval) from category 1 to 5 (denoted as C1-C5) at various translation speeds (*Uh*= 1,2,3,…10 m s-1). Region of self-induced cooling exceeding the 2.5°C threshold (from Emanuel, 1999) is shaded in grey, indicating unsuitable condition for intensification. (a) Estimation based on the climatological profiles (black profiles) along the typhoon tracks. (b) Estimation based on the *in situ* profiles (red profiles in Fig. 5) inside the positive-SSHA features.

Fig. 8: Pre-typhoon SSHA (in cm) maps and the tracks of the 22 gyre central cases (in chronological order, see also Table 3). Locations of the *in situ* profiles are depicted as green stars. The altimetry track is shown in yellow.
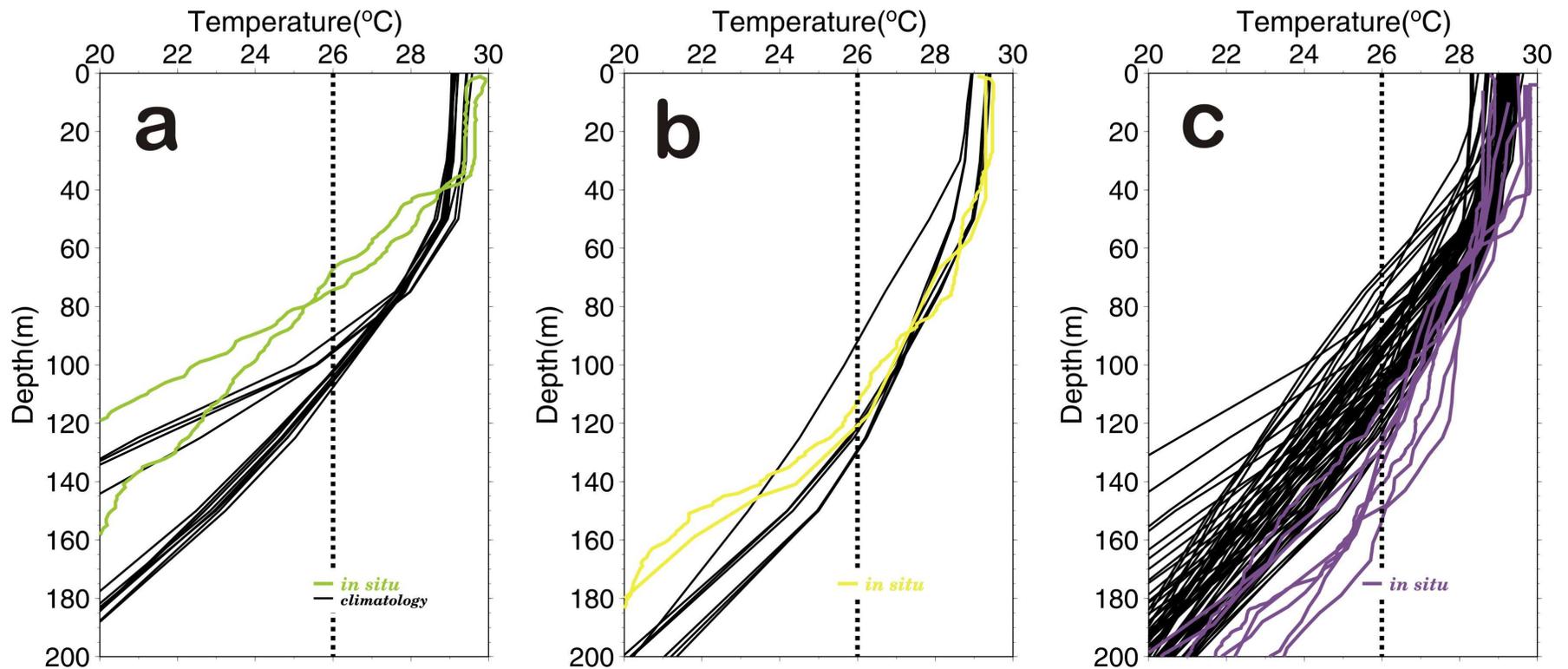
Fig. 9: *In situ* depth-temperature profiles (in color) .vs. the background climatological profiles (in black) for various scenarios in the gyre. (a) The negative-SSHA feature scenario. (b) The normal (no feature) scenario. (c) The positive-SSHA feature scenario. Locations of the *in situ* profiles are depicted as green stars in Fig. 7.
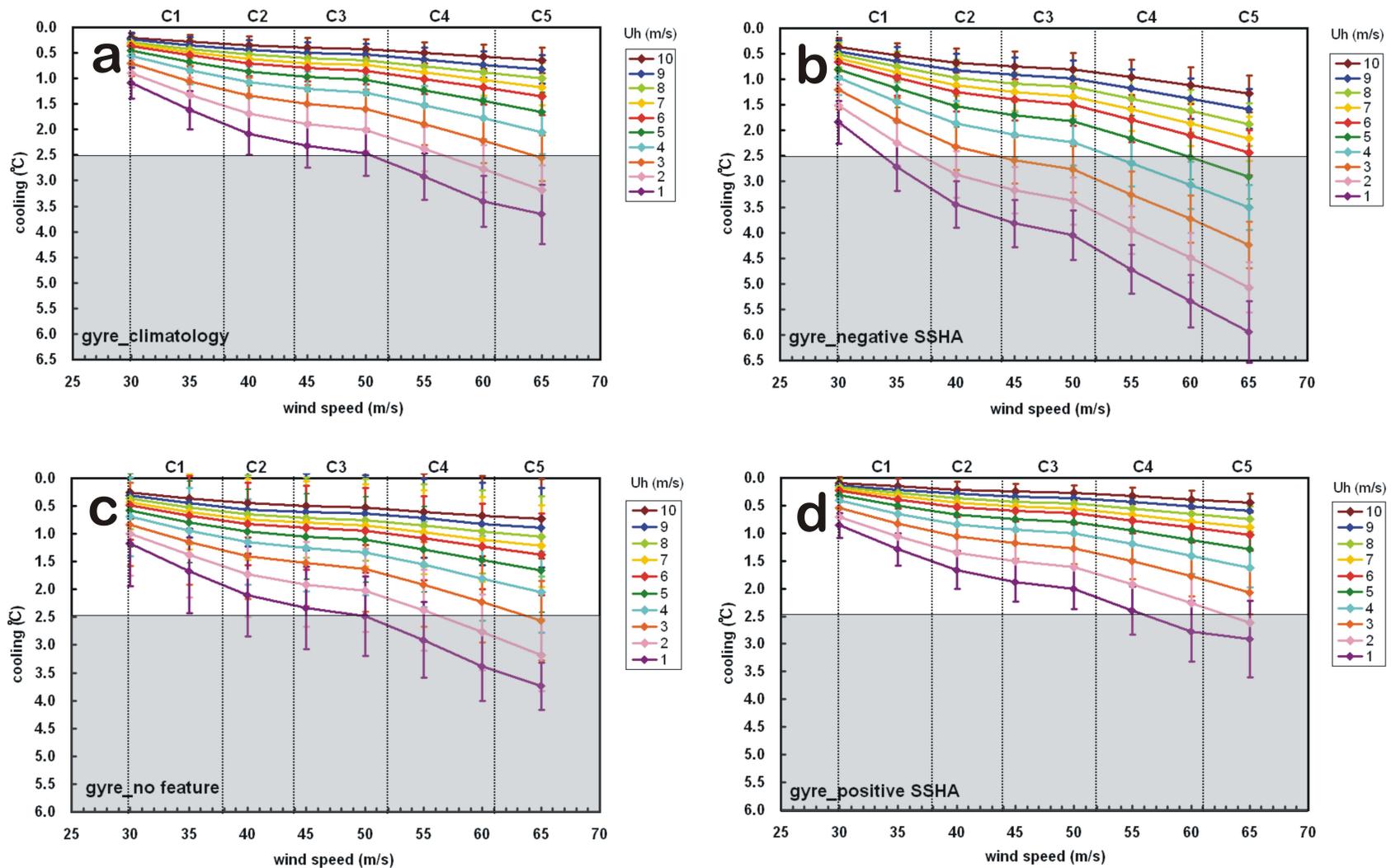
Fig. 10: As in Fig. 6, but for the self-induced ocean cooling estimation for the gyre cases. (a) Estimation based on the climatological profiles (black profiles) along the typhoon tracks. (b) Estimation based on the *in situ* profiles (green profiles in Fig. 8a) inside the negative-SSHA features. b) Estimation based on the *in situ* profiles (yellow profiles in Fig. 8b) under normal (no feature) condition. b) Estimation based on the *in situ* profiles (purple profiles in Fig. 8c) inside the positive-SSHA features.
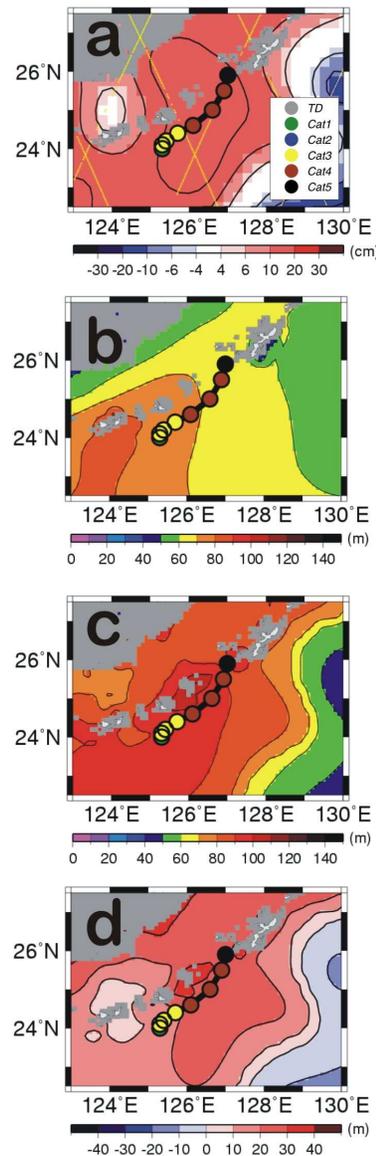
Fig. 11: The Kuroshio – positive SSHA feature case (i.e. Bart (1999), see also Table 3). (a) Pre-typhoon SSHA (in cm) map and the TC track. The altimetry track is shown in yellow. (b) The background climatological D26 from the NOAA/World Ocean Atlas (Stephens et al. 2002). (c) The positive-feature modulated D26, as estimated from a 2-layer reduced gravity ocean model proposed by Goni et al. (1996) and Shay et al. (2000). (d) The deepening of D26 by the positive SSHA feature (i.e., (c)) as compared with climatology (i.e., (b)).
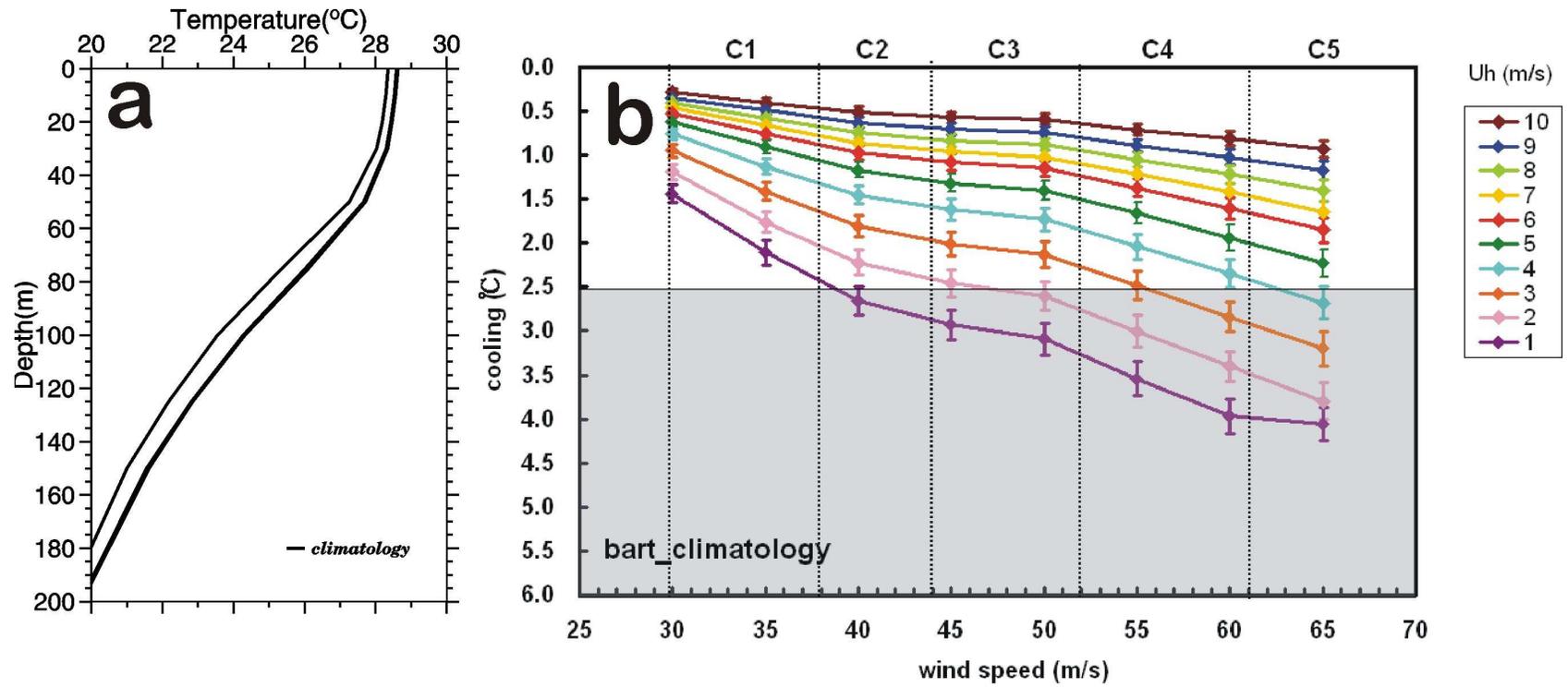
Fig. 12: (a) Climatological depth-temperature profiles along the track of typhoon Bart (1999). (b) As in Fig. 6, but for the self-induced ocean cooling estimation using the climatological profiles in (a).
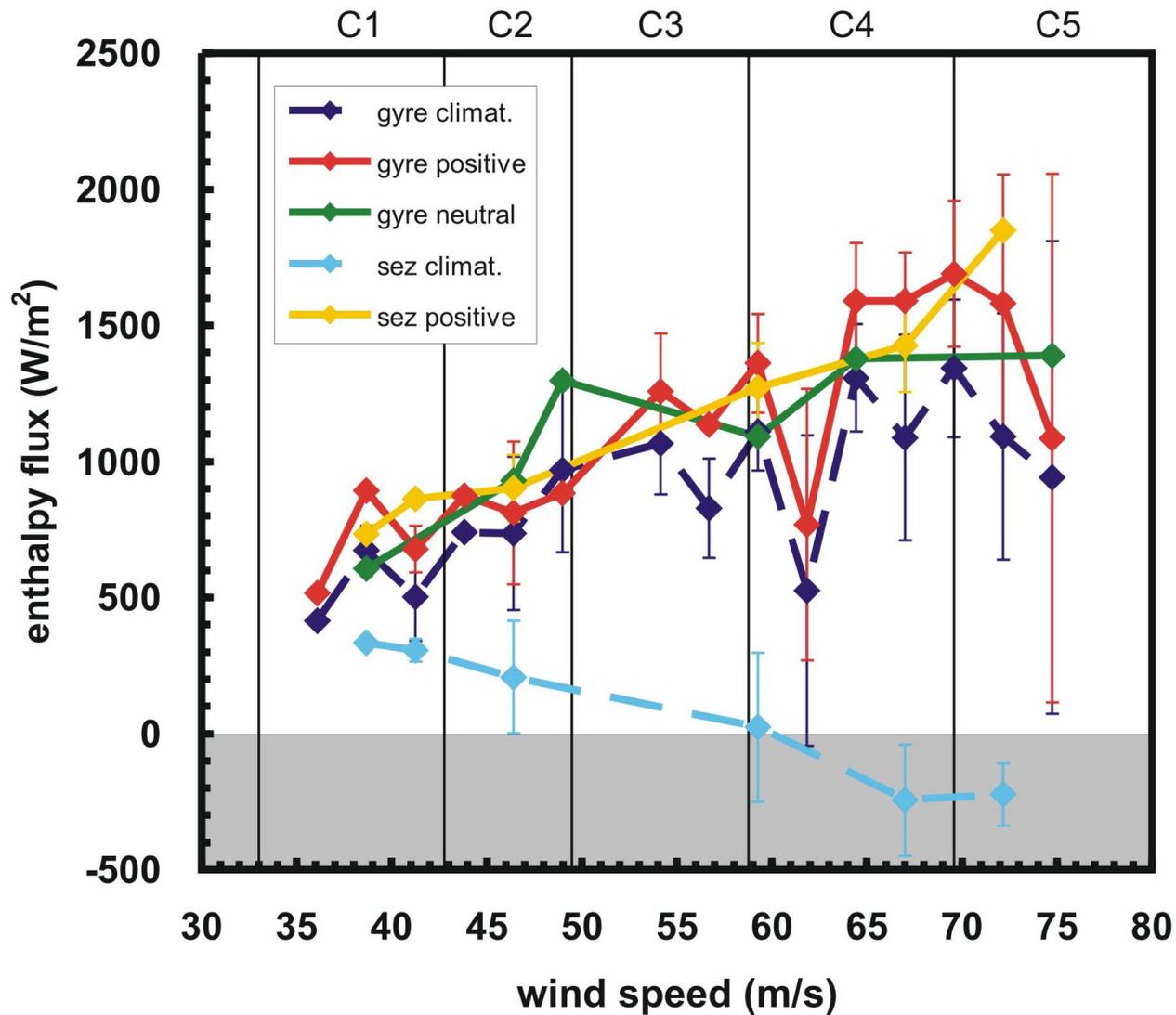
Fig. 13: The estimated available enthalpy (sensible + latent heat flux, in W m-2) during various stages of intensification for different scenarios: gyre climatology (blue dashed curve), gyre positive (red curve), gyre neutral (green curve), SEZ climatology (light-blue dashed curve), and SEZ positive (yellow curve).
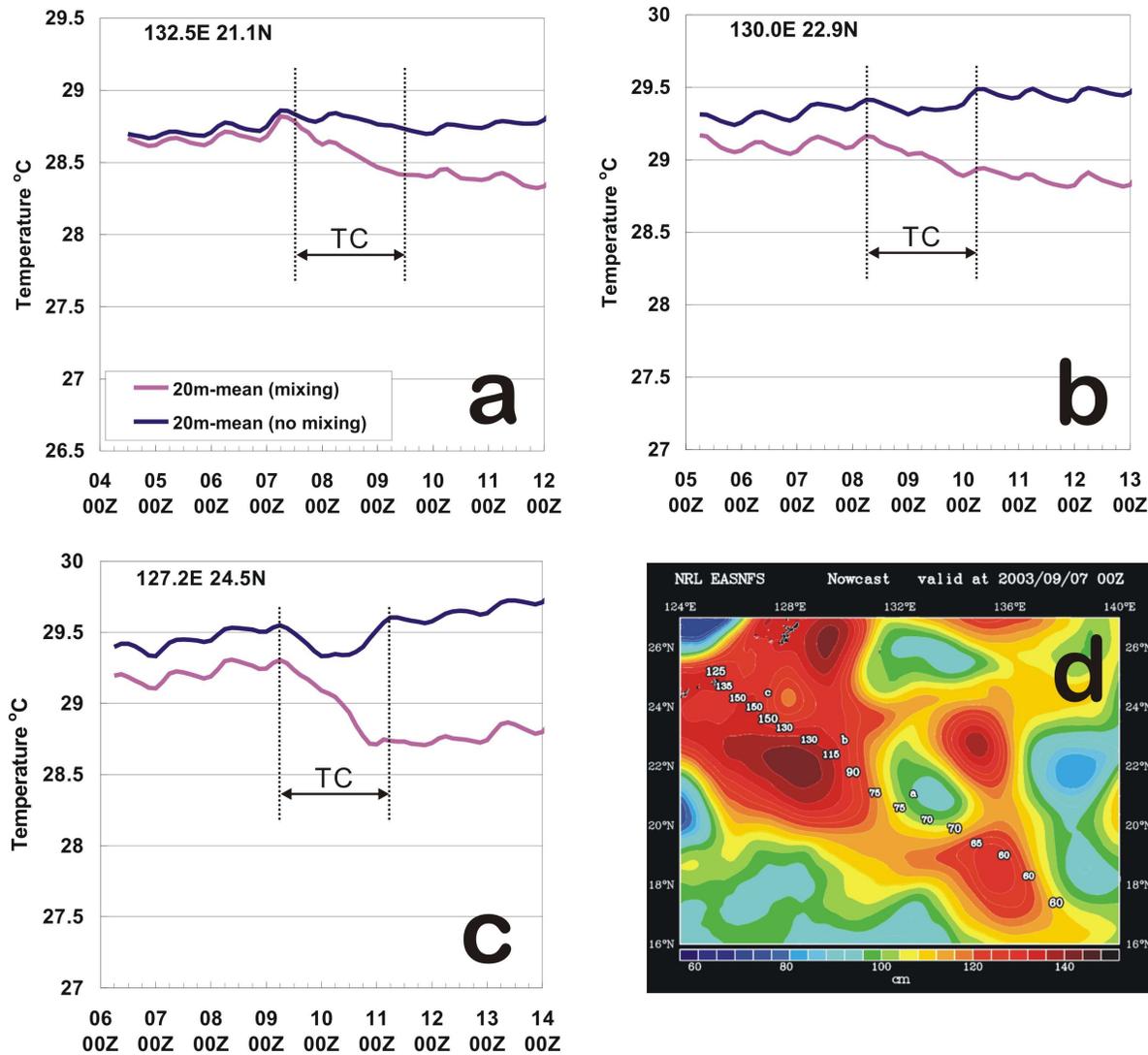
Fig. 14: 3-D numerical experiments using the US NRL's EASNFS ocean model showing upper ocean temperature evolution (average from surface to 20m depth) before, during, and after typhoon's passing for 3 locations. As shown in (d), Points b and c are located in the warm eddy while point a locates at the outside of the eddy. For each point, simulation is done with mixing (pink curves) and without mixing (blue curves).